Electronic Spectrum of Crystalline Antimony

P. J. Lin and J. C. Phillips+
Dept. of Physics and Institute of Metals
Univ. of Chicago, Chicago, Ill.

Abstract

The energy levels and interband oscillator strengths of antimony have been calculated at ~ 90,000 points in the Brillouin zone by the pseudopotential method. The potential used was obtained with no adjustment of parameters from empirical form factors of the semiconductors grey Sn and InSb. This potential had previously been used to obtain Fermi surfaces for electrons and holes in Sb in good agreement with experiment. The present calculation agrees well with optical data of Cardona and Greenaway in the energy interval 0.5 eV - 8.0 eV with E polarized perpendicular to the trigonal axis. Polarization effects of order 10 - 20% are predicted by the calculation. The regions of the Brillouin zone contributing most strongly to the calculated structure are identified, and predictions are made concerning spin-orbit splittings of the observed peaks. Application of the analysis to As, Bi, and IV - VI semiconductors is discussed.

1. Introduction

For many years the electronic properties of the group V semimetals As, Sb, and Bi have been the subject of extensive experimental investigation. Interpretation of the experiments was hampered in the past by lack of band calculations of sufficient accuracy and generality to establish the position and shape of the Fermi surfaces of electrons and holes in the Brillouin zone. Recently it has been shown that considerable progress towards interpretation of Fermi surface data can be made in Sb[1] and in As[2] by making use of empirical pseudopotentials derived from the very large amount of data available on the electronic structure of groups IV and III - V semiconductors. Thus in the case of Sb the pseudopotential form factor was obtained[1] from the known form factors of grey Sn[3] and InSb.[4] Without the introduction of any adjustable parameters the empirical form factor so derived from semiconductor spectra yielded surprisingly good quantitative agreement in the semimetals with detailed Fermi surface data obtained by cyclotron resonance[5] and de Haas-van Alphen experiments.[6]

We have been encouraged by these empirical successes to extend the calculations over a wider energy range and over the entire Brillouin zone in sufficient detail to obtain the optical spectrum in the range 0.5 - 15 eV. The data available in this range show only five or six

broad peaks, with little fine structure evident.[7] Over the same range considerably more structure is expected in the theoretical spectrum. Thus at present we cannot hope to achieve a comprehensive and exhaustive analysis of the spectrum of Sb to the degree that was achieved in Brust's classic work on Si and Ge.[8] The present work is therefore exploratory in character. With the development of modulated electro-reflectance[9] and piezo-reflectance[10] techniques of high resolution we hope that the details of the structure discussed here will become accessible to experiment, not only in the pure crystals but also in the alloy systems.

Because of the covalent character of the semi-metal crystal structure[11] even using the comparatively weak pseudopotential[1] for Sb one requires 90 plane waves to obtain convergent energy levels. Sampling these levels at a sufficiently large number of points in the primitive 1/12th of the Brillouin zone to obtain good statistics for spectral histograms would be prohibitively expensive if carried out directly, even in a pseudopotential representation. (We estimate that in standard orthogonalized plane wave or augmented plane wave calculations the cost would be 10 - 100 times greater still.) Economical techniques for handling the sampling problem have been developed by Brust.[8] We have refined his techniques somewhat, as described in Sec. 2.

In Sec. 3 we present the spectral histograms for $\underline{E}$ unpolarized and analyze the interband edges. The spectral histograms for $\underline{E}$ polarized || to the trigonal axis are analyzed similarly in Sec. 4. Comparison with experiment for Sb is made in Sec. 5, and the effects of spin-orbit interaction are discussed in Sec. 6. In Sec. 7 the spectrum of As is discussed and extension of the results to IV - VI semiconductors is considered.

2. Computational Techniques

In the Hartree or random phase approximation the imaginary part $\varepsilon_2(\omega)$ of the complex dielectric response is given in the notation of ref. 8 by

$$\varepsilon_2^{ij}(\omega) = \left(\frac{2\pi e}{m\omega}\right)^2 \hbar \sum_{n,s} \int_{B.Z.} \frac{2}{(2\pi)^3} \delta(\omega_{n,s}(\underline{k}) - \omega) \times | M_{n,s}^{i}(\underline{k}) M_{n,s}^{j}(\underline{k}) | d^3k \qquad (2.1)$$

where $M_{ns}^{i}(\underline{k})$ is the interband momentum matrix element

$$\hbar M_{ns}^{i}(\underline{k}) = \langle \psi_n(\underline{k}) | p^i | \psi_s(\underline{k}) \rangle \qquad (2.2)$$

The superscripts i, j describe the tensorial character of the dielectric response. The group V semimetals can be considered as two interpenetrating face-centered cubic lattices with a trigonal distortion of the rhombihedral angle γ from the value 60°. For Sb at 4.2°K we have

$\gamma \approx 57°$, so that the trigonal distortion is only 3°. Thus if there are any measurable polarization effects in the energy range considered we should expect to find them in the difference between $\varepsilon_2^{||}$ and $\varepsilon_2^{\perp}$, with $\underline{E}$ (or p^i in (2.2)) parallel or perpendicular to the trigonal axis. Because of the quasi-hexagonal symmetry in the basal plane polarization effects are assumed to be small there, as is found to be the case in infrared magneto-optic experiments.[12]

To evaluate $\varepsilon_2^{||}$ and $\varepsilon_2^{\perp}$ from (2.1) we have used the pseudopotential model.[1] In order to obtain convergence the model wave functions $\phi_n(\underline{k})$, which describe the Bloch functions $\psi_n(\underline{k})$ but with core oscillations omitted, are expanded to 90 plane waves. The resulting secular equation is then reduced to about 30 plane waves using the perturbation procedure described by Brust.[8] The kinetic cutoff energy E_N was chosen as 36.7 eV. With this choice of the cutoff the energy difference between E_N and free electron degeneracies at Γ, X, L and T was maximized, thus insuring minimum loss of symmetry due to reduction of the secular equation. Sampling at several values of $\underline{k}$ showed that this truncation procedure introduced errors in the eigenvalues of 0.1 eV or less.

Although the core terms are omitted from the model wave functions ϕ_n, in strongly covalent structures the replacement of $\langle \psi_n|\underline{p}|\ \psi_s\rangle$ by $\langle\phi_n|\underline{p}|\ \phi_s\rangle$ causes little

error at low energies because most of the oscillator strength from bonding to antibonding states lies in the region of interatomic overlap outside the atomic cores. This was demonstrated explicitly for Si in orthogonalized plane wave calculations,[13] and was confirmed in the pseudopotential calculations[8] for Si and Ge.

Because $\phi_n(\underline{k})$ has been expanded in plane waves calculation of $\langle\phi_n |\underline{p}| \phi_s\rangle$ is straightforward. For reasons of economy eigenvectors were obtained in terms of the first 20 reciprocal lattice vectors $\underline{K}_i$:

$$|\phi_n(\underline{k})\rangle \approx \sum_i c_i(n, \underline{k}) |\underline{k} + \underline{K}_i\rangle \qquad (2.3)$$

The oscillator strengths $p_{||}^2$ and $p_{\perp}^2$ were checked at symmetry points by comparison with selection rules obtained by group theory.

Next eigenvalues and oscillator strengths were calculated on a mesh of 250 points. The Brillouin zone is shown in Fig. 1 in terms of the trigonal reciprocal lattice vectors $\underline{g}_1, \underline{g}_2, \underline{g}_3$ defined previously.[14] By symmetry the mesh points $\underline{k} = h\underline{g}_1 + k\underline{g}_2 + \ell\underline{g}_3$ are confined to 1/12th of the zone specified by $k \geq \ell \geq h$ and $\ell \geq 0$. The sample of mesh points is too small to provide reliable statistics for our spectral histogram. Thus we generated by the Monte Carlo method[15] 7500 points in 1/12th of the zone and obtained eigenvalues and oscillator strengths at these points

by three-dimensional linear interpolation[16] according to the following formula:

$$f(\underline{r}) = \sum_i w_i f(\underline{R}_i) \Big/ \sum_i w_i \tag{2.4}$$

$$w_i = |\underline{r} - \underline{R}_i|^{-3} \tag{2.5}$$

where the points $\underline{R}_i$ include the eight points on the trigonal mesh nearest $\underline{r}$. The justification for the choice (2.5) of the weighting factors is the following. The probability P that a mesh point will fall at a distance $|\underline{r} - \underline{R}_i|$ is proportional to $|\underline{r} - \underline{R}_i|^2$. But with respect to $|\underline{r} - \underline{R}_i|$ linear interpolation requires that $W_i^{-1} = |\underline{r} - \underline{R}_i| P(|\underline{r} - \underline{R}_i|)$. This heuristic argument suggests that (2.4) and (2.5) could also be made slightly more accurate by extending the sum over more than the eight nearest neighbors on the mesh.

In the calculations presented below (2.1) is evaluated using $\underline{k}$-dependent oscillator strengths described by (2.2). In a preliminary calculation (2.1) was also evaluated with oscillator strengths for each pair of bands set equal to a constant C_{ns} independent of $\underline{k}$. The results of the two calculations were qualitatively similar, except that the $\underline{k}$-dependent calculation gave peaks in the optical spectrum which were narrower and higher. This suggests that the peaks are derived from transitions near symmetry points and symmetry lines, where the oscillator strength

for a given pair of bands is somewhat larger than its average value. This effect enhances spectral structure associated with peaks in the interband density of states derived from regions of high symmetry.

3. Unpolarized Spectrum

Broadly speaking the interband spectra of IV - VI semiconductors and V semimetals can be analyzed according to Cardona and Greenaway[7] into two groups. The lower group falls in the energy range 1 - 7eV and consists usually of three peaks, while the upper group falls in the range 5 - 15eV and always exhibits three peaks. The first group is labelled E_1 - E_3 and the second group is labelled E_4 - E_6. The results for the As-Sb-Bi family are particularly simple and are shown in Fig. 2 (after ref. 7) where the peak energies are plotted against lattice parameter.

Note that peak E_1 has not been identified in Sb, but that interpolation with respect to lattice constant places it at 1.5eV. Note also that the energy of peak E_2 (the largest peak in the spectrum) changes by a factor of 1.4 on going from As to Sb, while the (lattice parameter)$^{-2}$ changes only by a factor of 1.25. Thus the energy shifts are partly kinetic energy effects, but they also contain a term which scales like (lattice parameter)$^{-\alpha}$ with $\alpha > 3$, which is indicative of an effect associated with potential energies in the atomic cores.

The explanation for the two groups, according to Cardona and Greenaway,[7] is the following. The oscillator strength of the low energy group is derived from transitions between bonding and antibonding states, as in Ge. To study the high-energy group in more detail, one plots $\varepsilon_2 E^2$ against $E = \hbar\omega$. Then by comparing Ge and PbTe, as shown in Fig. 3, one sees that the high-energy group is virtually absent in Ge. It is associated with the ionic character of the crystal, and particularly with transitions between low-lying bonding s levels in the valence band and anti-bonding s and p levels in the conduction band just above E_F.

When peak energies are plotted against lattice parameter for PbS, PbSe, PbTe, SnTe and GeTe, a more complex pattern is obtained, as shown in Fig. 4 (after ref. 7). This pattern, however, provides further support for the idea that there is an important core contribution to the chemical shifts. Specifically relativistic core effects lower the energies of s bonding levels that are the dominant initial states for the group of high-energy peaks. As noted by Phillips,[17] in Fig. 4 when only the anion is varied (solid lines) the interband energies decrease with increasing lattice parameter. The absolute decrease associated with core effects is about twice as rapid for the higher energy group as for the lower energy group.

Because of relativistic effects s levels in Pb are more tightly bound than in lighter elements, a fact confirmed both spectroscopically by atomic term values and chemically by the divalence of Pb in chemical reactions. Thus the shift of the high energy group, which originates from s-like cation levels, is expected, for with increasing lattice constant the Pb atoms fill a decreasing fraction of the volume of the unit cell, thus binding s levels less tightly. When only the cation is varied (dashed lines), a reverse trend is found, as expected when Pb is replaced by lighter elements with less tightly bound s levels. Finally, the smaller shift of the low energy group compared to the high energy group indicates that the bonding $\longrightarrow$ antibonding transitions in the 1-7 eV range are less affected by hybridization of s-like states in the valence band, and thus have predominantly p character.

The generality of the foregoing discussion of chemical shifts is both appealing and disappointing. In order to assign particular peaks to particular bands and particular regions of the Brillouin zone, as was done[8] for Si and Ge, it is necessary to carry out detailed band calculations. The results obtained from the energy bands[1] shown in Fig. 5 by averaging over all orientations of $\underline{E}$ relative to crystal axes and summing over all pairs of bands are shown in Fig. 6. Two main peaks are found in $\varepsilon_2 E^2$ located at 2.2 eV (labelled

E_2) and 5.1 eV (labelled E_4). There is a subsidiary peak (labelled E_5) at 6.8 eV and weaker peaks are seen at 9.2, 10.9 and 12.6 eV.

The theoretical oscillator strengths at higher energies are considerably weaker than the experimental oscillator strengths. This is almost certainly caused by the fact that the initial and final states are well separated in the nearly free electron approximation; the oscillator strength for higher energy transitions is chiefly associated with the core terms, which have been omitted in our calculation. However, the states of greatest interest are those near the Fermi energy interest are those near the Fermi energy which contribute to the spectral structure below 7 eV. We therefore focus our attention on this region.

Structure in interband optical spectra arises because there are regions in $\underline{k}$ space where the valence and conduction bands are nearly parallel. Associated with each of these regions are one or more critical points defined by

$$\nabla_{\underline{k}} \left[E_c(\underline{k}) - E_v(\underline{k}) \right] = 0 \qquad (3.1)$$

A single critical point produces the usual asymmetric edges. Two or more quasi-degenerate saddle-point edges of opposite types produce a peak (see Fig. 1 of ref. 8).

In cubic crystals such as Ge and Si where most of the

oscillator strength is concentrated in a single pair of bands, the number of strong interband edges may be so small that most of the important edges are resolved in the spectrum of a single crystal. In a given case some edges may be marked by stronger edges, but can be separated and observed in other crystals of the same family. Moreover, the topology of the bands may be such that a peak produced by two quasi-degenerate edges remains in spite of substantial chemical shifts, because the two edges move together (e.g., the 4.4 eV peak in Ge and Si is seen also in many III-V and II-VI zinc-blende crystals).

The situation in the semi-metals is different. Because the crystals are distorted by only a few degrees from fcc symmetry, a number of interband edges split into quasi-degenerate edges. Moreover as shown in Fig. 5 the crystal potential is such that at L and T (which are equivalent to the point L in fcc crystals) near E_F there are six levels distributed over a band of energies 2.5 eV wide near E_F (which is to be compared with 5 levels spread over more than 5 eV in Si and Ge at L[8]). At Γ in the conduction band from 3 to 5.5 eV above E_F there are also six levels. Only at X and W are the levels sparcely spaced.

Because of the small energy denominators members of a group of closely spaced levels at a symmetry point repel

one another strongly as one leaves the symmetry point. Thus the critical points at Γ, L and T are not expected to contribute strongly to structure in the fundamental absorption region. However, there is ample evidence[7,18,19] that the direct absorption edge E_o at around 0.3 eV in PbTe, PbSe and PbS occurs at L. Thus we would expect that the Sb band edges identified at 0.10 and 0.14 eV in magneto-optic studies[12] should be associated with transitions from or to the Fermi surface near L or T. (The detailed ordering of the levels at these points will not significantly affect the optical spectrum in the energy range we are considering; however the ordering shown in Fig. 5, while not necessarily unique, is compatible with Fermi surface data.[1])

Other interband critical points may be found along symmetry lines. Removal of crossover degeneracies in the free electron approximation produces kinks, e.g., between Γ and X, which were previously tentatively identified with interband edges in the spectra of the Pb salts.[7,19] However the present calculations show both that the phase space associated with these kinks is small and that they do not fall at energies close to peaks in the interband density of states for the pair of bands in question. This emphasizes the importance of detailed sampling of $\underline{k}$ space for the interpretation of optical data.

Because of the large number of critical points present in the spectrum we have followed Brust's procedure[8] and decomposed the complete spectrum into a superposition of spectra from pairs of bands. Bands $4 \rightarrow 6$ and $5 \rightarrow 6$ are shown in Fig. 7 and Fig. 8 and bands $5 \rightarrow 8$ and $5 \rightarrow 9$ are shown in Fig. 9. From the pair spectra we conclude that peak E_2 is associated with $4 \rightarrow 5$ and $4 \rightarrow 6$ transitions, peak E_3 with $4 \rightarrow 5$, $4 \rightarrow 6$ and $4 \rightarrow 7$ transitions, and peak E_4 with $(4,5) \rightarrow (8,9,10)$ transitions.

Consider peak E_3 in the $4 \rightarrow 6$ and $5 \rightarrow 6$ spectra. The leading edge in the $5 \rightarrow 6$ spectrum falls at 5.10 eV and is readily identified with an M_1 type saddle point belonging to $X_4 \rightarrow X_1$. Within the accuracy of our calculation X_3 is degenerate with X_4: the splitting of these levels caused by the trigonal crystal field is smaller than 0.03 eV. However the leading edge of peak E_3 in the $4 \rightarrow 6$ spectrum is displaced to 5.25 eV, because the interband critical point has moved to the point A shown in Table I. This shows that although the rhombohedral splitting of the X levels is small, the same splitting of the interband edge is 0.15 eV, because in the crystal of lower symmetry one of the interband critical points has moved slightly away from X. The movement in $\underline{k}$ space, i.e., the distortion of the shape of the interband energy surface, produces a far larger crystal field splitting of the edge than of the states at the sym-

metry point. Displacement of critical points has been mentioned as an important source of structure in piezoreflectance experiments,[20] and the behavior of the $(X_3, X_4) \rightarrow X_1$ edge supports this suggestion.

Presumably the E_3 peak in the $5 \rightarrow 6$ spectrum is produced by a combination of M_1 and M_2 saddle points. The M_2 saddle point associated with the higher edge is difficult to locate because its energy is close to that of the M_1 edge; we believe it falls near U, and the transition is near $U_1 \rightarrow U_1$. The higher edge in the $4 \rightarrow 6$ spectrum is marked B in Fig. 7; it is associated with $U_2 \rightarrow U_1$ transitions.

The E_2 peak is prominent in the $5 \rightarrow 6$ and $4 \rightarrow 6$ spectra, with peaks at 2.0 and 2.4 eV, respectively. No edge structure is evident, and none of the critical point energies derived from symmetry points or lines fit the peak energy. From a survey of the points contributing to these histograms we have concluded that for both $4 \rightarrow 6$ and $5 \rightarrow 6$ transitions peak E_2 arises from critical points in the general volume of the zone near $\underline{g} = \underline{k} = (0.59, -0.43, 0.08)$. A curious feature of the points contributing to the $4 \rightarrow 6$ and $5 \rightarrow 6$ histogram E_2 peaks is that many of them fall in same region of $\underline{k}$ space with a splitting of about 0.3 eV. We return to this point later in connection with spin-orbit effects.

The E_5 peak at 6.8 eV is derived primarily from $5 \rightarrow 9$ transitions, as shown in Fig. 8. It appears to be produced by M_1 and M_2 type critical points near Γ T = Λ. We have not located these critical points, but we list in Table I and show in Fig. 5 the position of an interband transition along Γ T which accounts for the polarization effects discussed in the following section.

4. Polarized Spectrum.

We have evaluated (2.1) using $|\langle n|\underline{p}|s\rangle|^2$ for the oscillator strength, giving ε_2 with $\underline{E}$ unpolarized, and also using $3|\langle n|p_t|s\rangle|^2$, where p_t is the component of $\underline{p}$ along the trigonal axis, from which we obtain $\varepsilon_2^{||}$. At first sight with a distortion in Sb of only 3° from cubic, one might expect polarization effects to be small. However, even at Γ states of p character that would have been three-fold degenerate in cubic symmetry are split by as much as 0.5 eV by the rhombohedral distortion. Moreover the displacement of critical points away from symmetry points, lines and planes by the cubic distortion appears after to have opposite effects for pairs of bands with oscillator strengths strongly polarized parallel or perpendicular to the trigonal axis, leading to a separation of parallel and perpendicular oscillator strengths over an energy range two or three times

greater than the crystal field splitting of the Γ levels. This tendency[21] has been noted previously in connection with polarized studies[22] of the reflectivity of zinc-blende and wurtzite crystals (cubic and hexagonal symmetry, respectively).

The spectrum of $\varepsilon_2^{\parallel}E^2$ is shown in Fig. 6 together with $\varepsilon_2 E^2$(unpolarized). There are strong polarization effects accompanied by alternation of intensities: peaks E_2 and E_5 are stronger with $\underline{E}$ parallel to the trigonal axis, while peak E_4 is weaker. To establish the origin of these polarization effects, we also show the results for $\varepsilon_2^{\parallel}$ in Fig. 7 ($4 \rightarrow 6$ transitions), Fig. 8 ($5 \rightarrow 6$ transitions) and Fig. 9 ($5 \rightarrow 8,9$ transitions). Peaks E_2 and E_4 are polarized in $4 \rightarrow 6$ but not in $5 \rightarrow 6$ transitions. Comparing the results listed in Table II with those shown in Fig. 7 and Fig. 8 we see that there is general agreement between the polarization behavior at the critical points and in the histograms, except that the polarization of $X_4 \rightarrow X_1$ does not significantly enhance the polarization of the E_4 peak in the $5 \rightarrow 6$ histogram. On the other hand, the region near Λ presumably accounts for the polarization of the E_5 peak in the $5 \rightarrow 9$ histogram, which is why this point along Λ is listed in Table I even though the associated critical points are

displaced somewhat from the Λ line.

5. Comparison with Experiment.

The experimental data[7] were taken with $\underline{E} \perp$ trigonal axis. We obtain $\varepsilon_2^{\perp} E^2$ from Fig. 6 and in Fig. 10 plot it against the experimental values[23] obtained by Kramers-Kronig transformation of the reflectance. Below 8 eV the agreement between experiment and theory is remarkably good. Note that peak E_1, which is resolved in As and in Bi, is not seen in the Sb spectrum. Also peak E_3 in the original reflectance spectrum is weak and is lost when the Kramers-Kronig transform is taken to obtain ε_2. As shown in Fig. 7 there is weak structure in our histograms which might be associated with E_3 in the reflectance spectrum, but we prefer not to attach that much significance to our calculation. Similar remarks apply to peak E_6. The strong peaks E_2, E_4 and E_5 agree with experiment far better than was anticipated, considering the exploratory character of the calculation.

6. Spin-Orbit Effects.

In view of the remarkable agreement between theory and experiment exhibited in Fig. 10, we now examine the results of our calculation critically. Polarization effects of order 10-20% should be observable. If we now add a spin-orbit term

$$H_{SO} = \lambda \underline{L} \cdot \underline{S} \qquad (6.1)$$

to the Hamiltonian, what will its effect be on the spectral structure shown in Fig. 10?

Specifically peak E_4 is identified with $(4,5) \rightarrow (6,7)$ transitions near X and K. The low-energy edge of E_4 associated with $5 \rightarrow 6$ transitions is marked $X_4 \rightarrow X_1$ in Fig. 8 and that associated with $4 \rightarrow 6$ transitions is marked A in Fig. 7. The separation of 0.15 eV between $X_4 \rightarrow X_1$ and A is small compared to the spin-orbit parameter $\lambda = 0.6$ eV in Sb. Thus when (6.1) is included by perturbation theory the low-energy edge of peak E_4 should show a spin-orbit splitting similar to those exhibited by $\Lambda_3 \rightarrow \Lambda_1$ edges in the diamond-and zinc blende-type crystals.[8] In spite of lifetime broadening this splitting may be detectable by derivative techniques at low temperatures.

Because the initial and final states are non-degenerate no splitting is expected of E_5. Whether peak E_2 should split or not is difficult to say. The E_2 peaks in the $4 \rightarrow 6$ and $5 \rightarrow 6$ histograms are separated by less than 0.3 eV (orbital splitting). As noted in section 3, many of the same volume points contribute both to the $4 \rightarrow 6$ and $5 \rightarrow 6$ E_2 peaks and are separated by as little as 0.2 eV. These states (unlike X_3 and X_4) do not have definite p atomic character, but are part s and part p, so that the spin-orbit splitting will be only a fraction of λ. Thus a splitting in Sb may

be difficult to detect. In Bi, on the other hand, with λ = 1.5 eV the doublet structure observed in reflectivity at 1.2 and 1.7 eV and marked E_1?, E_2 by Cardona and Greenaway[7], does correspond to the magnitude of the spin-orbit effect that would be expected on the basis of our calculations.

7. Application to As and to IV - VI Semiconductors.

There are two qualitative differences between Sb and As. The distortion angle $\delta = 60° - \gamma$, where γ is the rhombohedral angle, is about 3° in Sb and 6° in As. Also the spin-orbit parameter λ is about 0.2 eV in As. This means that orbital splittings of edges that would have been degenerate in the cubic structure are likely to be larger in As than Sb. When this is combined with a reduced value of λ it seems unlikely that spin-orbit splittings of either E_2 or E_4 should be observable in As.

As an example consider the peak E_4. Theoretical and experimental edge energies are shown for this peak for Sb and for As in Table II; the theoretical values for As were obtaining using the pseudopotential described previously[2]. At first sight the shift of the reflectance peak of 1.2 eV from 5.7 to 6.9 eV on going from Sb to As appears to be in poor agreement with the change in energy of 0.5 eV of $X_4 \rightarrow X_1$ from the pseudopotential calculations. However, the energy at B changes by 1.6 eV. This indicates that increase of

the trigonal distortion should broaden E_4. The reflectance data for As have not been transformed by Kramers-Kronig methods, but the width of the E_4 reflectance peak does seem to be about 50% greater in As than in Sb in qualitative agreement with our expectations.

Our assignment to specific regions of $\underline{k}$ space of the interband peaks is most firm for peak E_4, which we assign to the X and K neighborhoods. Because of the striking similarities of the IV - VI and V spectra we believe this assignment should also be valid for the IV - VI semiconductors. In the case of PbTe the spin-orbit splitting of the X_3 and X_4 levels (X_5, in the cubic single group, $X_6^- + X_7^-$ in the cubic double group) has been calculated[18] to be 0.9 eV, and the transitions $X_6^- \rightarrow X_1$ and $X_7^- \rightarrow X_1$ are found at 5.3 and 6.2 eV, respectively, compared with an experimental value of 6.2 eV. Ordinarily the interband curvature of the lower of a pair of spin-orbit doublets is much less than that of the higher, leading to much greater oscillator strength for the lower, heavy mass edge. Thus the values to be compared are the theoretical value of 5.3 eV and the experimental value of 6.2 eV. The values so obtained are similar to those shown in Table I for Sb, with the experimental value about 0.7 eV greater than the theoretical one in both cases. The general simi-

larity of the PbTe bands obtained by the augmented plane wave method[18] to the Sb bands obtained by the pseudopotential method[1] and to the PbTe bands obtained empirically[19] is reassuring.

8. Conclusions.

With this survey of the optical data we have shown that the energy bands of As and Sb obtained by the pseudopotential method from form factors of the elements yield good agreement with Fermi surface data and with optical data over a range in energy from 0.5 to 8.0 eV. The form factors of the elements in turn were obtained empirically from semiconductor spectra, and for our purposes contained no adjustable parameters. Should the exploratory calculations described here and in previous papers[1,2] prove to be correct we shall have succeeded in determining the electronic structure of the lighter semi-metals empirically from the known electronic structure of the simpler cubic semiconductors. This approach, which has already yielded good results[24] for Mg_2X with X = Si and Ge, appears to represent a universal empirical method for obtaining the electronic structure of crystals which do not contain transition, rare-earth, or noble metals.

The calculations presented here make simple predictions concerning polarization effects and spin-orbit splittings

which it should be possible to test experimentally. As noted by Cardona and Greenaway,[7] the effects of lifetime broadening are greater in the semimetals than in semiconductors, but it should be possible to overcome these using recently developed derivative techniques.[9,10]

We are grateful to Prof. L. M. Falicov for discussions of the material presented here.

REFERENCES

1. L. M. Falicov and P. J. Lin, Phys. Rev. (in press).
2. P. J. Lin and L. M. Falicov, Phys. Rev. (in press).
3. P. J. Lin and J. C. Phillips, Advances in Physics (in press).
4. M. L. Cohen and T. K. Bergstresser, Phys. Rev. (in press).
5. W. R. Datars and J. Vanderkooy, IBM, J. Res. Develop. 8, 247 (1964).
6. L. R. Windmiller and M. G. Priestley, Solid State Communications 3, 199 (1965).
7. M. Cardona and D. L. Greenaway, Phys. Rev. 133, A1685 (1964).
8. D. Brust, Phys. Rev. 134, A1337 (1964).
9. B. O. Seraphin and R. B. Hess, Phys. Rev. Letters 14, 138 (1965).
10. W. E. Engeler, H. Fritzsche, M. Garfinkel and J. J. Tiemann, Phys. Rev. Letters 14, 1069 (1965); G. W. Gobeli and E. O. Kane, Phys. Rev. Letters 15, 142 (1965).
11. M. H. Cohen, L. M. Falicov and S. Golin, IBM, J. Res. Develop. 8, 215 (1964).
12. M. S. Dresselhaus and J. G. Mavroides, Phys. Rev. Letters 14, 259 (1965).

References (continued)

13. L. M. Kleinman and J. C. Phillips, Phys. Rev. 118, 1153 (1960).

14. L. M. Falicov and S. Golin, Phys. Rev. 137, A871 (1965).

15. D. Brust, Phys. Rev. 139, A489 (1965).

16. When (2.4) and (2.5) are used in one-dimension they are equivalent to smoothing the final histogram by Simpson's rule. In three dimensions, however, (2.4) and (2.5) strongly smooth the histogram even though only linear interpolation is used. Another interesting question is the number n of Monte Carlo points that should be used per mesh point. This was determined by requiring that 99% of the mesh points have at least one Monte Carlo point nearest them, which requires that $8(7/8)^n = 0.01$ giving $n \approx 50$.

17. J. C. Phillips, Solid State Physics, Vol. 18 (ed. F. Seitz and D. Turnbull), Academic Press, New York (in press).

18. J. B. Conklin, Jr., L. E. Johnson and G. W. Pratt, Jr., Phys. Rev. 137, A1282 (1965).

19. P. J. Lin and L. Kleinman, Phys. Rev., (in press).

20. U. Gerhardt, Phys. Rev. Letters, 15, 401 (1965).

References (continued)

21. J. C. Phillips, Phys. Rev. 133, A452 (1964).

22. M. Cardona and G. Harbeke, Phys. Rev. 137, A1467 (1965).

23. We are grateful to Prof. M. Cardona for communicating his original values of $\varepsilon_{\frac{1}{2}}$.

24. P. M. Lee, Phys. Rev. 135, A1110 (1964).

FIGURE CAPTIONS

Fig. 1. The Brillouin zone of Sb. The basic volume sampled in our calculations constituting 1/12 of the volume of the zone is bounded by the interior planes Γ LL', Γ LUT, Γ L'XT, and the surface planes of the zone. For a more detailed description of the crystal and Brillouin zone structure, see ref. 14.

Fig. 2. Shifts of interband peaks and edges in the As - Sb - Bi family (after Cardona and Greenaway) plotted against lattice parameter.

Fig. 3. Shifts of interband peaks and edges of IV - VI semiconductors (after Cardona and Greenaway) plotted against lattice parameter.

Fig. 4. Comparison of $\varepsilon_2 E^2$ in PbTe and Ge (following the notation of Cardona and Greenaway). According to the detailed calculations presented here, peak E_2 in Ge corresponds to peak E_5 in PbTe as well as in the semi-metals. On the other hand, peaks E_1, E_2 and E_3 in PbTe have no simple analogue in the Ge spectrum.

Figure Captions (continued)

Fig. 5. The energy bands of Sb as calculated using the present pseudopotential and as described in ref. 1. Interband arrows have been drawn indicating the approximate location of regions contributing to the peaks shown in Table I.

Fig. 6. The calculated values of $\varepsilon_2 E^2$ in Sb in $(eV)^2$ for unpolarized light and for $\underline{E}$ polarized parallel to the trigonal axis using the band structure which is partially described in Fig. 5. Three major peaks are resolved and these appear to correspond to peaks E_2, E_4 and E_5 in the notation of Cardona and Greenaway.

Fig. 7. The $4 \rightarrow 6$ contribution to the complete spectrum shown in Fig. 6. The letters A and B refer to neighborhoods shown in Table I. We label by E_3? structure which might correspond to the E_3 peak of Cardona and Greenaway, but which is too weak for positive identification.

Fig. 8. The $5 \rightarrow 6$ contribution to the complete spectrum shown in Fig. 6. Note that the polarization effects which were large in the $4 \rightarrow 6$ spectrum shown in Fig. 7 are negligible in the $5 \rightarrow 6$ spectrum.

Figure Captions (continued)

Fig. 9. The $5 \rightarrow 8$ and $5 \rightarrow 9$ spectra in the region of the E_5 peak.

Fig. 10. Comparison of theoretical and experimental spectra with $\underline{E} \perp$ trigonal axis. Note that the scale of the theoretical spectrum has not been adjusted. The experimental data are from Cardona and Greenaway (ref. 7). The correspondence at lower energies between the three main peaks E_2, E_4 and E_5 is good. At higher energies the theoretical oscillator strengths are too small, probably because of the omission of core terms. It is also possible that the experimental values of $\varepsilon_2 E^2$ are too large at higher energies (especially above 10 eV) where the rate at which $\varepsilon_2 \rightarrow 0$ may not be given accurately by the Kramers-Kronig transforms.

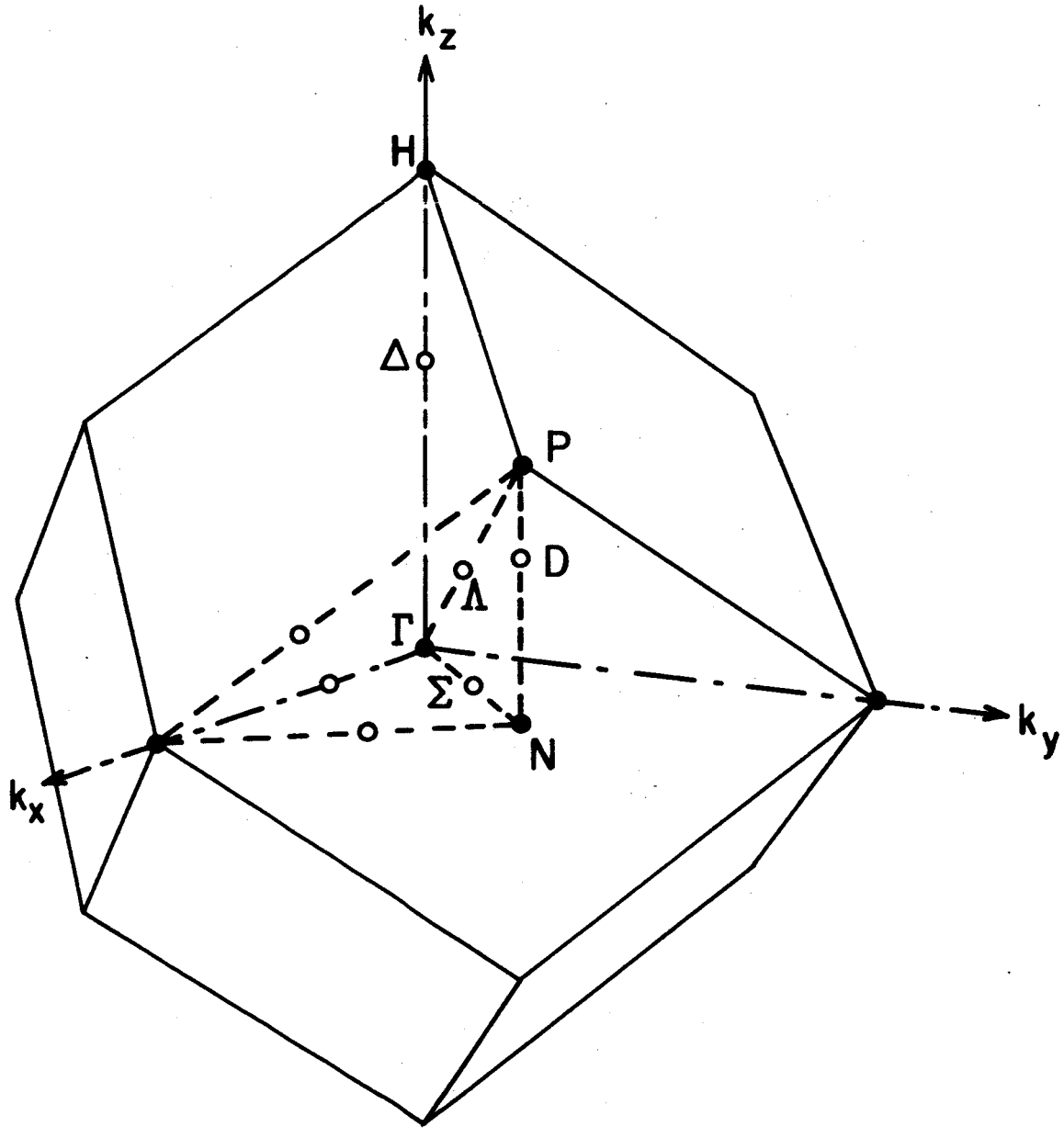

Fig. 1

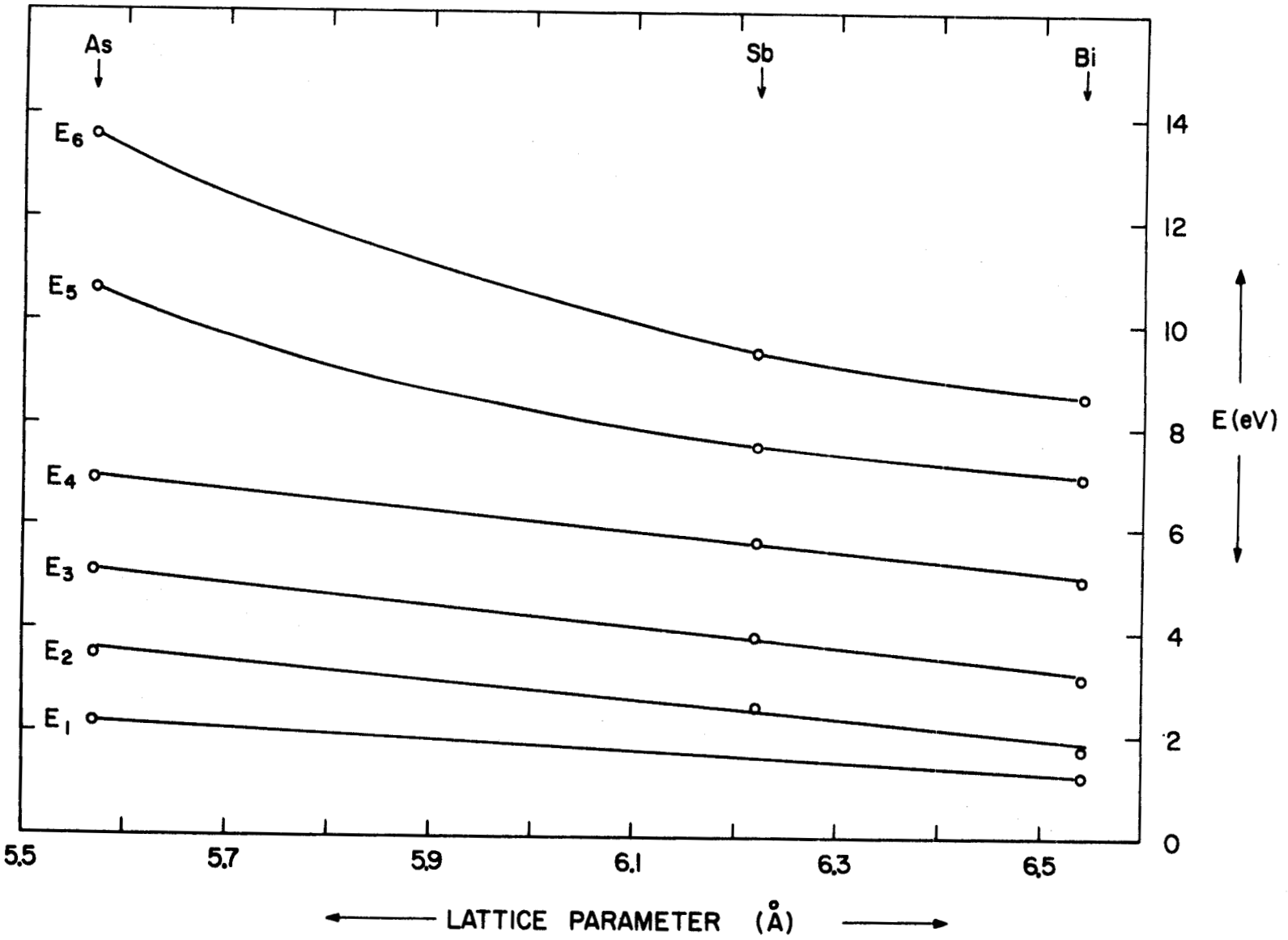
As
Sb
Bi
E6
E5
E4
E3
E2
E1
14
12
10
8
6
4
2
0
E (eV)
5.5
5.7
5.9
6.1
6.3
6.5
LATTICE PARAMETER (Å)

Fig 2

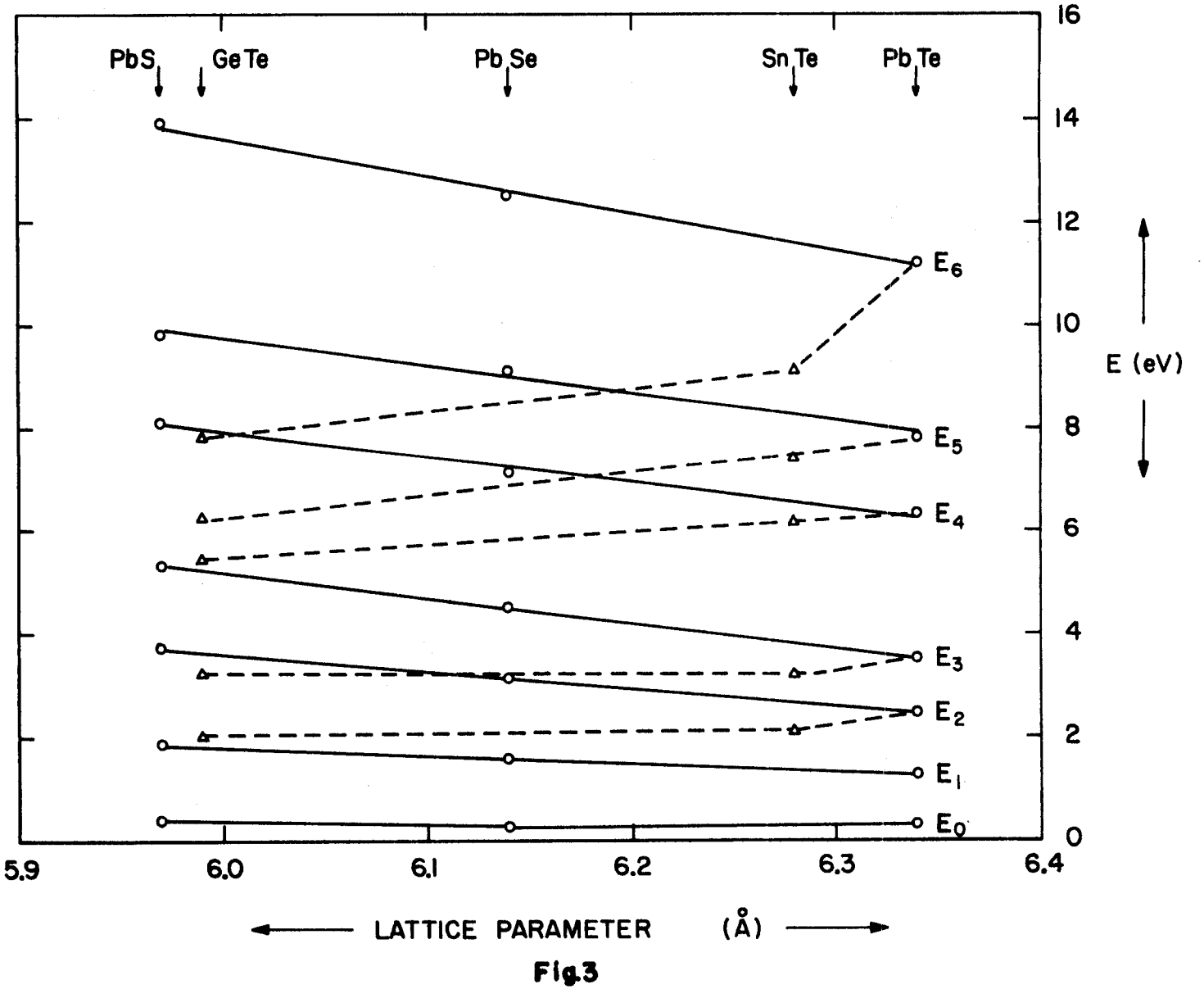
PbS
GeTe
PbSe
SnTe
PbTe
E6
E5
E4
E3
E2
E1
E0
16
14
12
10
8
6
4
2
0
E (eV)
5.9
6.0
6.1
6.2
6.3
6.4
LATTICE PARAMETER (Å)

Fig.3

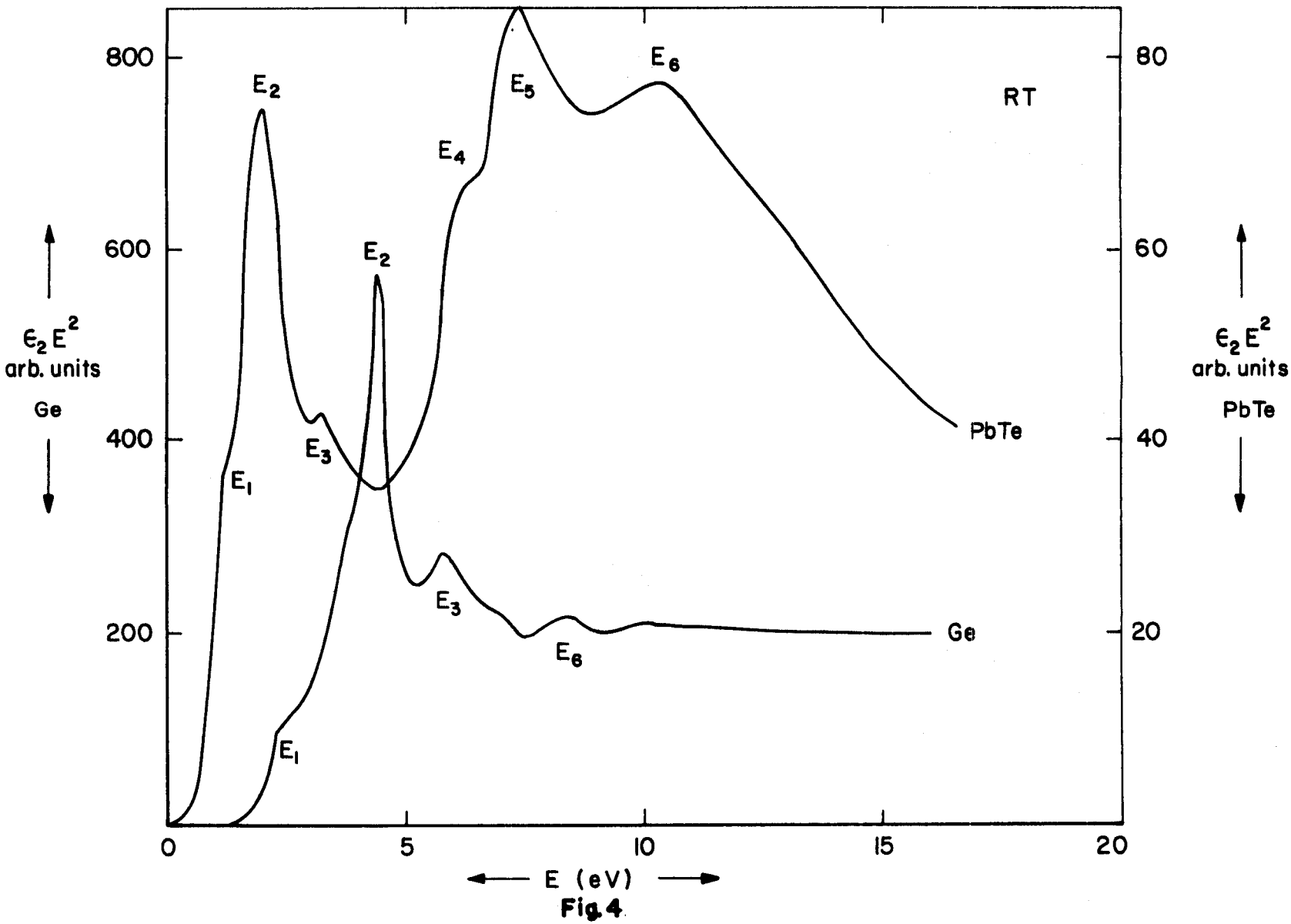
800
600
400
200
80
60
40
20
0
5
10
15
20
E (eV)
$\epsilon_2 E^2$ arb. units
Ge
$\epsilon_2 E^2$ arb. units
PbTe
RT
PbTe
Ge
E_1
E_2
E_3
E_4
E_5
E_6
E_1
E_2
E_3
E_6

Fig. 4

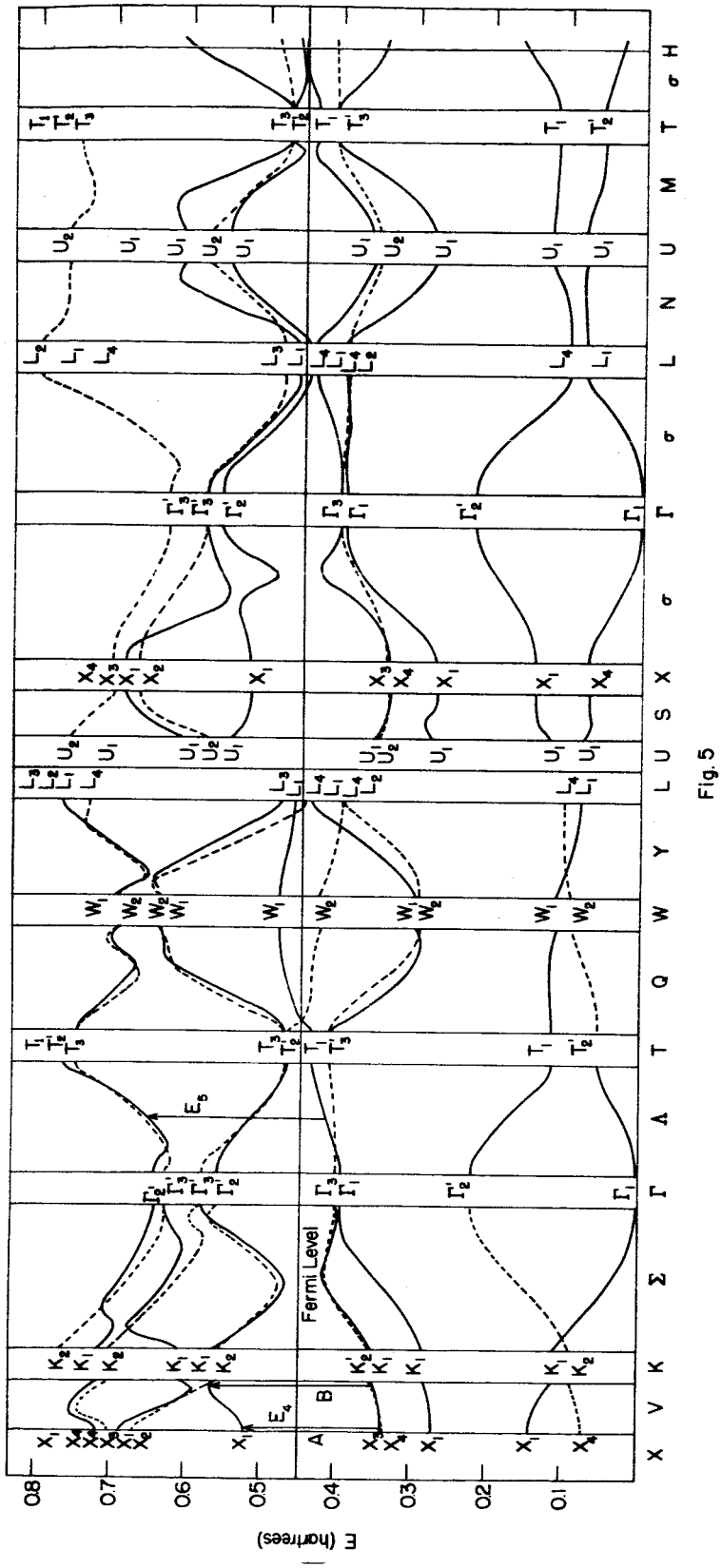
E (hartrees)
0.8
0.7
0.6
0.5
0.4
0.3
0.2
0.1
Fermi Level
A
B
X V K Σ Γ Δ T Q W Y L U S X σ Γ σ L N U M T σ H
E_4
E_5

Fig.5

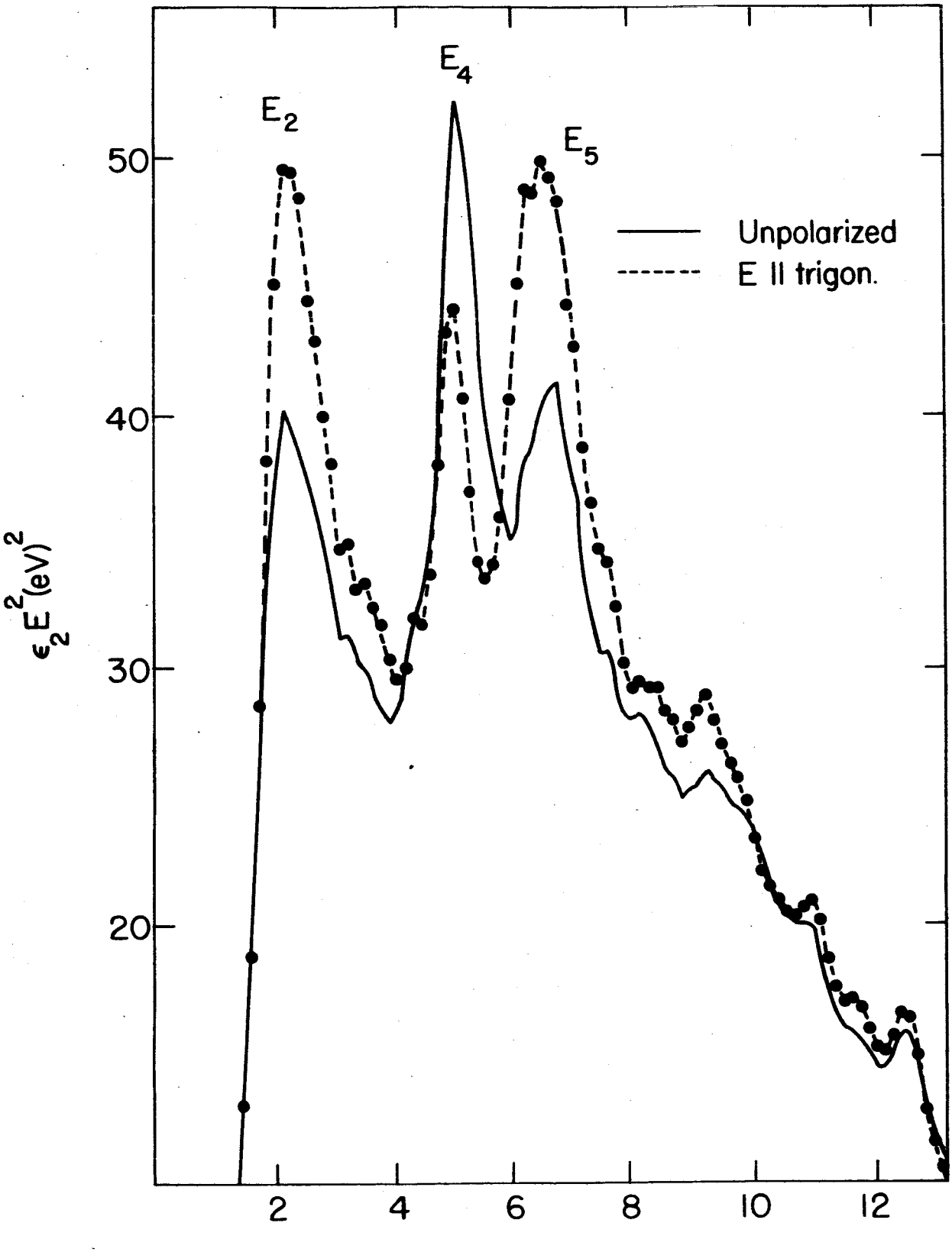
E2
E4
E5
50
40
30
20
Unpolarized
E II trigon.
$\epsilon_2 E^2(eV)^2$
2
4
6
8
10
12
E (eV)

Fig. 6

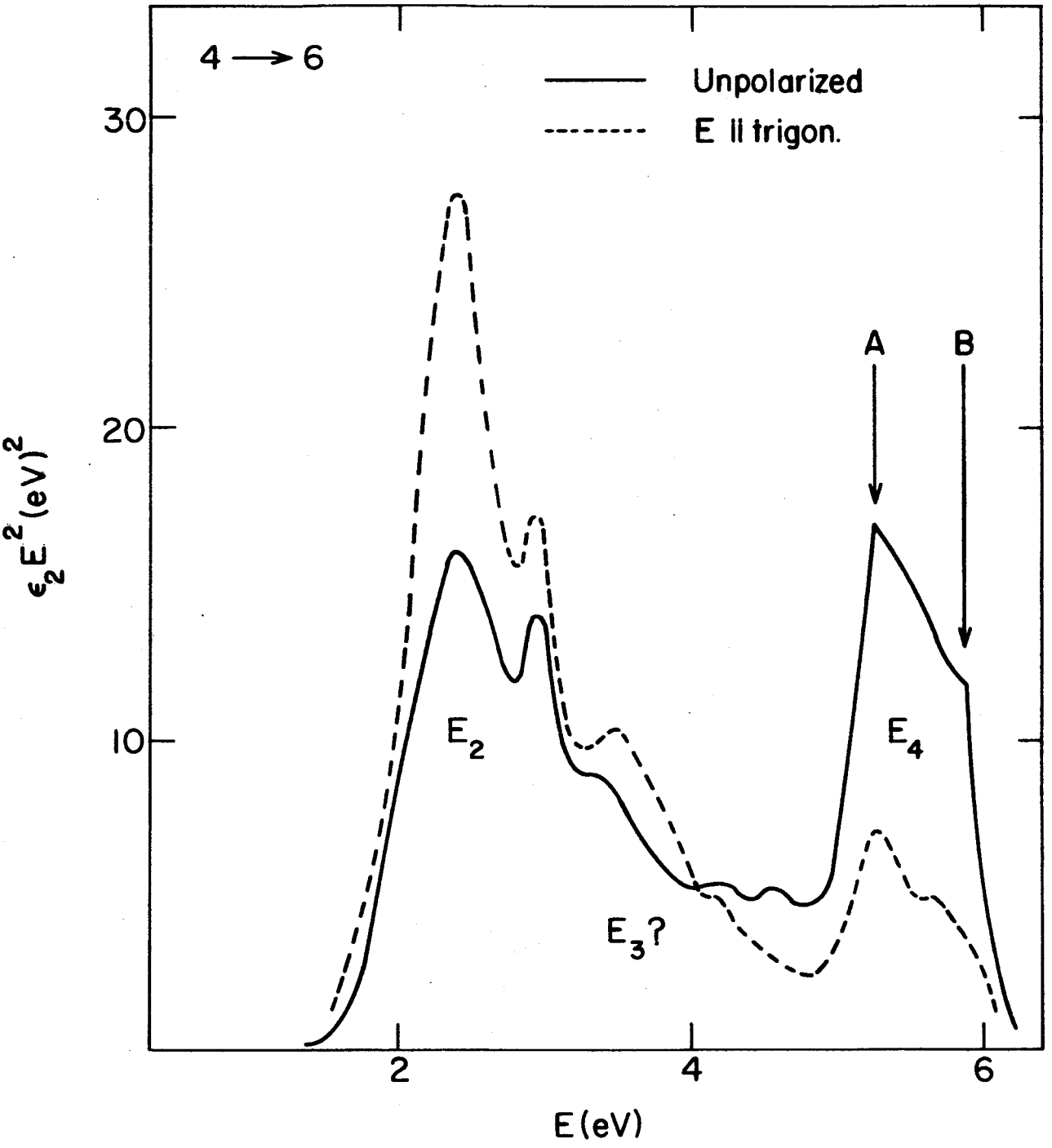
4 → 6
Unpolarized
E ll trigon.
30
20
10
$\epsilon_2 E^2 (eV)^2$
A
B
E_2
E_4
E_3?
2
4
6
E(eV)

Fig. 7

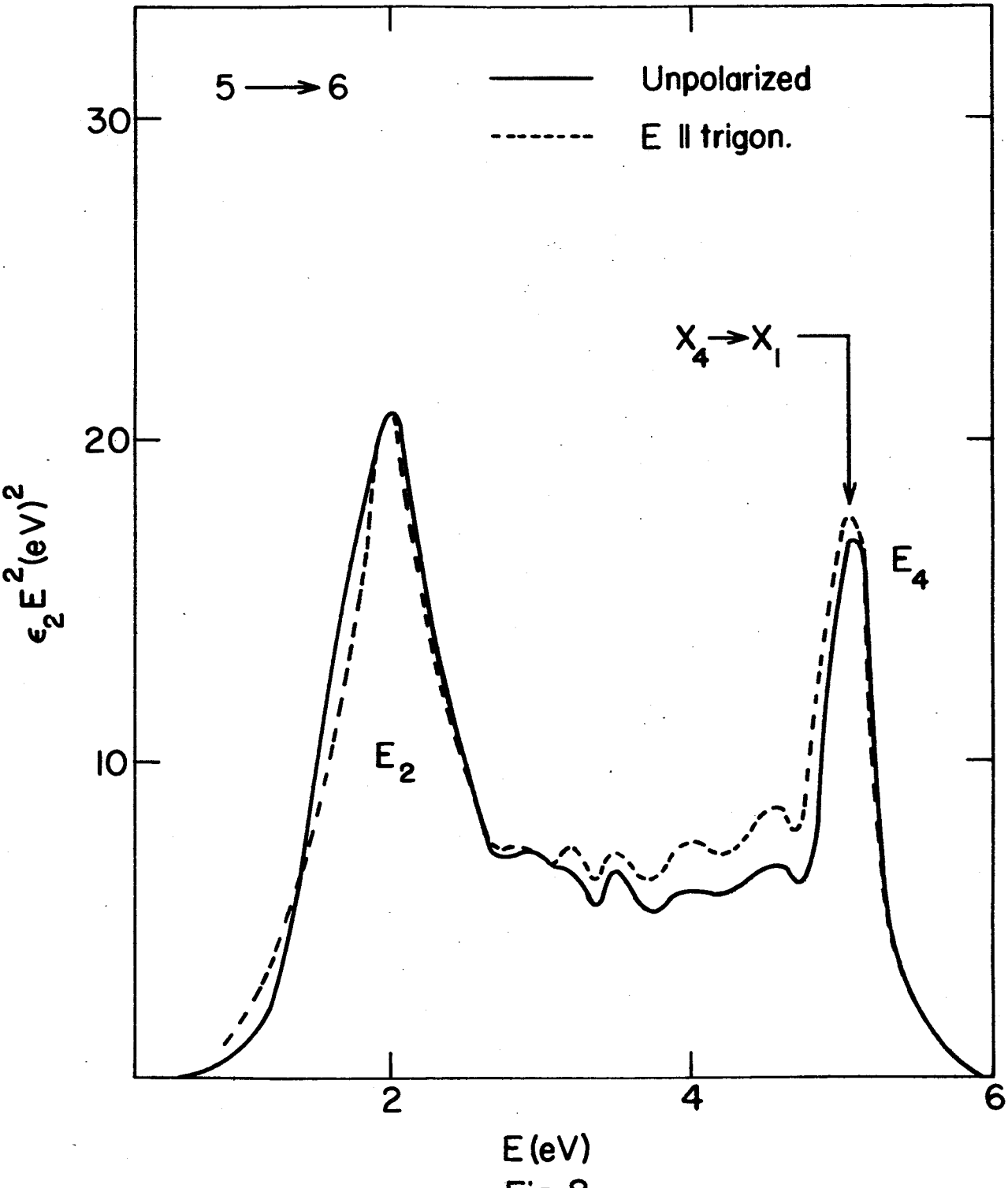

Fig. 8

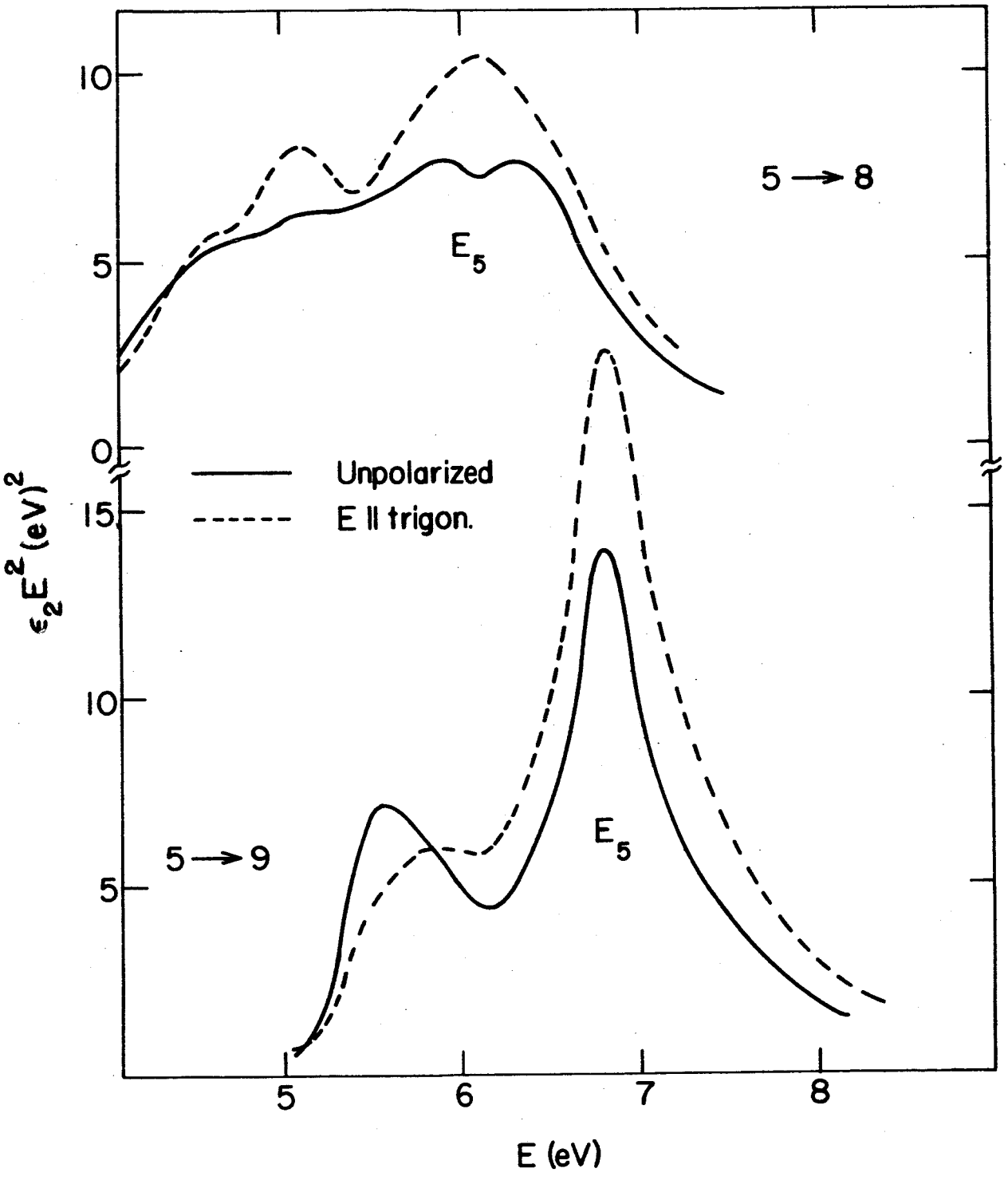
10
5
0
15
10
5
5 → 8
E5
Unpolarized
E ll trigon.
5 → 9
E5
5
6
7
8
E (eV)
ε2E2 (eV)2

Fig. 9

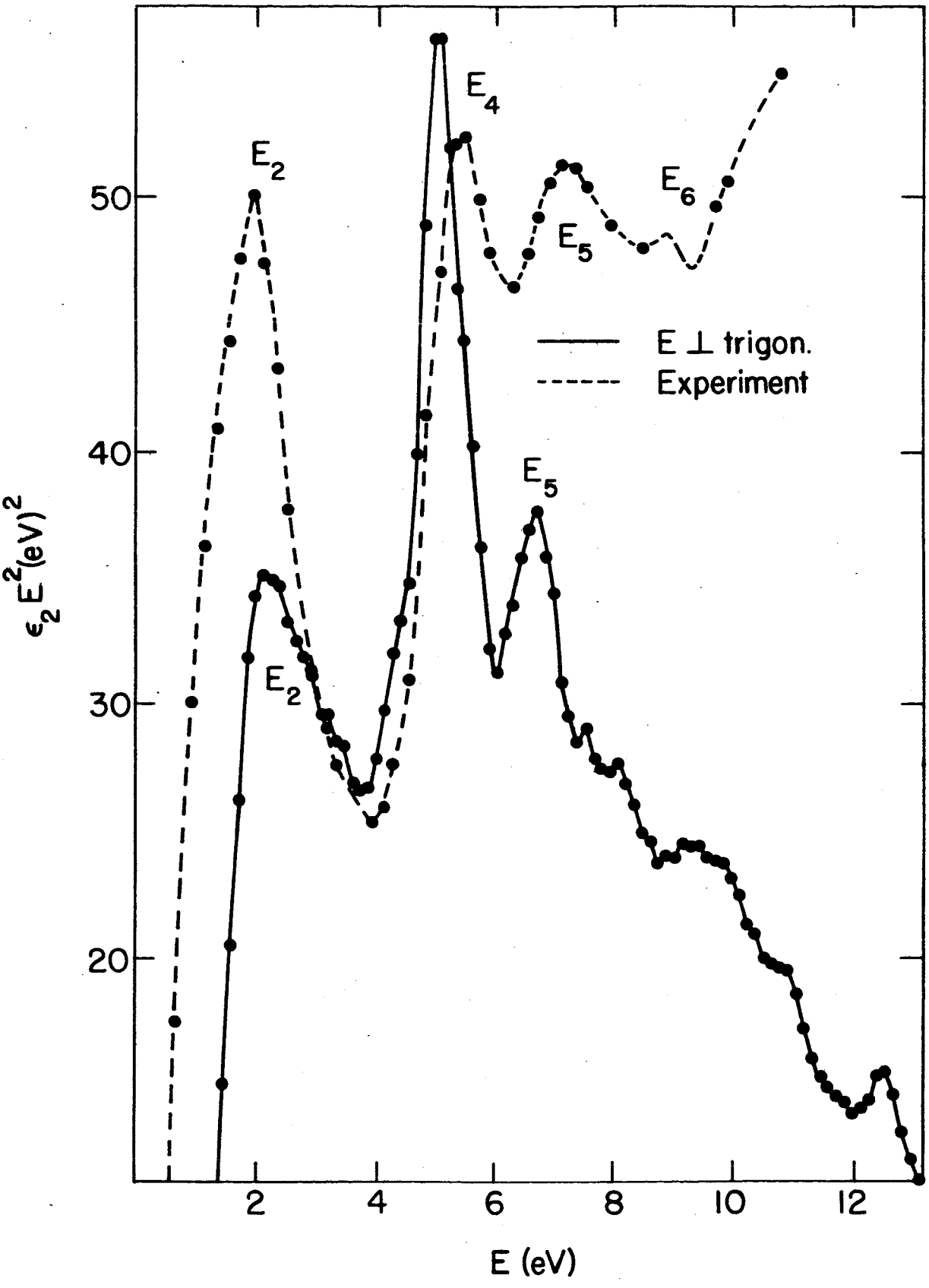
E4
E2
E6
E5
E ⊥ trigon.
Experiment
E5
E2
50
40
30
20
2
4
6
8
10
12
$\epsilon_2 E^2(eV)^2$
E (eV)

Fig. 10

Location	Bands	Symbol	Energy(eV)	Av.Os. Strength	‖Os. Strength
(1, -0.02, -0.02)	5 → 6	$X_4 \rightarrow X_1$	5.10	0.22	0.42
(1, -0.02, -0.02)	4 → 6	$X_3 \rightarrow X_1$	5.10	0.32	<0.15
(0.92, -0.10, 0.06)	4 → 6	A	5.25	0.26	<0.15
(1.0, -0.19, 0.15)	4 → 6	B	5.8	0.26	<0.15
(0.24, 0.24, 0.24)	5 → 9	$\Lambda_1 \quad \Lambda_1$	6.6	0.18	.54

Table I. Description of energies and polarizations of interband critical points. The oscillator strengths are given in arbitrary units in order to indicate the extent of polarization effects.

Element	$X_4 \rightarrow X_1$	B	$\varepsilon_2 E^2$	Center E_4	Width
Sb	5.1	5.8	5.6	5.7	0.7
As	5.6	7.4	--	6.9	1.1

Table II. Comparison of two interband energies in eV at X and B (see Table I) in As and Sb, as calculated theoretically. The maximum in the theoretical value of $\varepsilon_2 E^2$ in Sb is listed. Also the centers and widths of the E_4 reflectance peak as measured by Cardona and Greenaway for Sb and As are shown in the last two columns.